Co-clinical photon counting CT research for multi-contrast imaging

C. T. Badea[1], D.P. Clark[1], A. Alphin[1], J. C. Ramirez-Giraldo[2], P. Bhandari[3],
Y. M. Mowery[4], K. B. Ghaghada[3]

[1] Quantitative Imaging and Analysis Lab, Dept. of Radiology, Duke University Medical Center, Durham, NC
[2]Siemens Healthineers, Cary, NC 27511

[3]Singleton Dept. of Radiology, Texas Children's Hospital/Baylor College of Medicine, Houston, TX 77030

[4]Dept. of Radiation Oncology, Duke University Medical Center, Durham, NC 27710

Abstract

Developing novel contrast agents for multi-energy photon-counting (PC)CT will require a clear translation pathway from preclinical validation to clinical applications. To begin this development, we have used a clinical PCCT scanner (Siemens NAEOTOM Alpha) to study the spectral separation of a few contrast elements (Iodine, I; Gadolinium, Gd; Hafnium, Hf; Tantalum, Ta; Bismuth, Bi; Calcium, Ca) with currently available scanning protocols (fixed: 120 kVp, 20 and 65 keV thresholds). We also explored the capabilities of clinical and preclinical PCCT to image mice with sarcoma tumors injected with nanoparticles (NP). Our results indicate that Ta or Hf are complementary to I or Gd, providing excellent spectral separation for future multi-agent studies. Based on preclinical PCCT with four energy thresholds, we also conclude that additional energy thresholds will benefit clinical PCCT. Furthermore, we demonstrate the role that multi-channel denoising and reconstruction algorithms will play in pushing the bounds of spatial and spectral resolution with clinical PCCT. Performing co-clinical research will facilitate the translation of novel imaging algorithms and NP contrast agents for PCCT.

Keywords: x-ray CT (CT), photon counting, small animal imaging (SMAX)

*cristian.badea@duke.edu; phone 1-919-684-7509; https://sites.duke.edu/qial/

INTRODUCTION

Photon-counting detectors (PCD) can significantly improve CT contrast and enable quantitative material separation with a single CT scan. Because of these advantages, the maturation of PCCT technology promises to enhance routine CT imaging applications with high-fidelity spectral information. This enhancement has been demonstrated in large animal [1] and rabbit [2] studies using prototype clinical hardware. Our group has advanced preclinical PCCT by building prototype systems and demonstrating their value in cancer [3] and cardiac [4] studies in mice. The full potential of PCCT has not yet been realized, since it is dependent on the development and clinical translation of new contrast agents. Here, we investigate spectral separation of high Z element contrast materials using PCCT, and we demonstrate a co-clinical paradigm for PCCT research to translate preclinical validation experiments to clinical applications [5].

METHODS

1.1 Clinical PCCT

A phantom (Fig. 1) containing solutions of various contrast elements was prepared using a stock solution of 10 mg/mL elemental standard to prepare subsequent dilutions (Iodine, I; Gadolinium, Gd; Hafnium, Hf; Tantalum, Ta; Bismuth, Bi; Calcium, Ca). Dilutions were prepared in 2% nitric acid. For imaging studies, solutions were filled in 50 mL centrifuge tubes in concentrations of 10, 5, 2.5, 1.25, and 0.625 mg/mL. Our experiments used an FDA-approved clinical PCCT system (Siemens *NAEOTOM Alpha*) installed at Duke. The scans were performed at 120 kVp with a spiral pitch of 0.8 and used two fixed energy thresholds at 20 and 65 keV. The dose was 16 mGy. The phantom and mouse images were reconstructed with a dual-energy (DE) protocol using a Qr40 kernel and a voxel size of 0.29x0.29x0.4 mm, which yielded 70 keV virtual monoenergetic CT images (VMI) and two binned images (low energy, 20-65 keV; high energy, 65-120

7th International Conference on Image Formation in X-Ray Computed Tomography,
edited by Joseph Webster Stayman, Proc. of SPIE Vol. 12304, 123040G
 · 0277-786X · doi: 10.1117/12.2646399

keV). The reconstructed matrix size was 512x512. The reconstructed data was also decomposed on the scanner to create I maps overlaid on virtual non contrast (VNC) images. The binned images allowed alternative material decompositions.
A second *ex vivo* mouse scan was performed to achieve higher spatial resolution (0.15x0.15x 0.2 mm, kernel Qr 98u). The radiation dose was increased to 64 mGy to reduce noise. The scanner reconstructed 70 keV VMI images, but does not currently reconstruct separate bin images or perform material decomposition for this high resolution scanning mode. For both the high and low resolution clinical images we performed post-reconstruction denoising using our rank-sparse kernel regression algorithm[6].

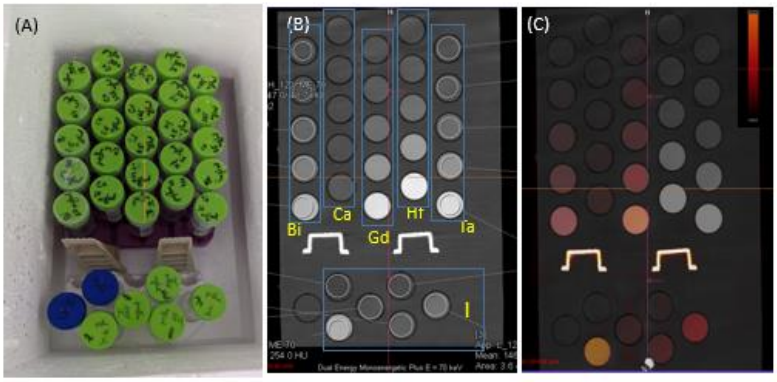

Figure 1: The elements phantom: (A) a photo, (B) CT image corresponding to VMI at 70 keV and showing measurement ROIs, and (C) the iodine decomposition map (red) overlaid on top of the VNC image. Note that the I map also shows positive enhancement for Gd, Bi, and Ca; however, the Hf and Ta vials are clearly separated from I.

1.2 PC Micro-CT

Our PC micro-CT system contains two imaging chains based on using both an energy-integrating detector and a PCD [3]. Each chain uses a G-297 X-ray tube (Varian Medical Systems, Palo Alto, CA) with a 0.3 mm focal spot size powered by an Epsilon high-frequency X-ray generator (EMD Technologies, Quebec, Canada). For this work, we have used only the imaging chain with a SANTIS 1604 CdTe-based PCD developed by Dectris, Ltd. (www.dectris.com). This detector has 150-µm pixel size and four energy thresholds. The source-to-detector distances were 831 and 680 mm, giving a magnification of approximately 1.2. To extend the PCD field-of-view along the z-axis and to reduce ring artifacts in our reconstructions, the subject was placed on a translational stage, and scans were performed using a helical trajectory. Our selection of kVp (120) and energy thresholds (20, 34, 50 and 65 keV) was based on the clinical scanner settings. The first and the last threshold (20 and 65 keV) were selected to match the clinical thresholds, while the other two were intended to match I (33.2 keV) and Gd (50 keV) K-edges. We used 200 ms exposures and 1 mA for each projection and 900 projections at each threshold. Based on ionization chamber measurements, the absorbed radiation dose was ~100 mGy. The projection data were air normalized, and the gaps between the tiles of the PCD were filled via interpolation.

Image Reconstruction: We performed an iterative reconstruction using the split Bregman method with the add-residual-back strategy [7] and rank-sparse kernel regression regularization (RSKR,[6]), solving the following optimization problem: and solved the following optimization problem:

$$\mathrm{X} = \underset{\mathrm{X}}{\arg\min} \tfrac{1}{2}\textstyle\sum_e \|\mathrm{R}\mathrm{X}_e - \mathrm{Y}_e\|_2^2 + \lambda\|\mathrm{X}\|_{\mathrm{BTV}}. \qquad (1)$$

This algebraic reconstruction problem solves for the vectorized, reconstructed data, the columns of X, for each energy threshold simultaneously (indexed by *e*). The reconstruction for each threshold minimizes the reprojection error (R, system projection matrix) relative to the log-transformed projection data acquired at each threshold (the columns of Y). To reduce noise in the reconstructed results, this data fidelity term is minimized subject to the bilateral total variation (BTV) measured within and between energies via RSKR.

1.3 Material Decomposition

Extending the approach of Alvarez and Macovski [8], we performed post-reconstruction spectral decomposition both on clinical PCCT and PC micro-CT data. On the clinical DE PCCT data, we studied the following basis material decomposition: a) I and Ca, b) I and Gd and c) I and Ta. Using the PC micro-CT data we have performed a) I and Gd decomposition using 20 and 65 keV threshold images (unsubtracted) and b) photoelectric effect (PE), Compton scattering (CS), I and Gd decomposition using all 4 thresholds images. Vials of known concentrations of each material were used to construct a sensitivity matrix of enhancement per unit concentration (HU/mg/mL). Spectral decomposition was then

performed by matrix inversion, followed by sub-space projection to prevent negative concentrations. After decomposition, the material maps were color coded and combined in ImageJ for visualization.

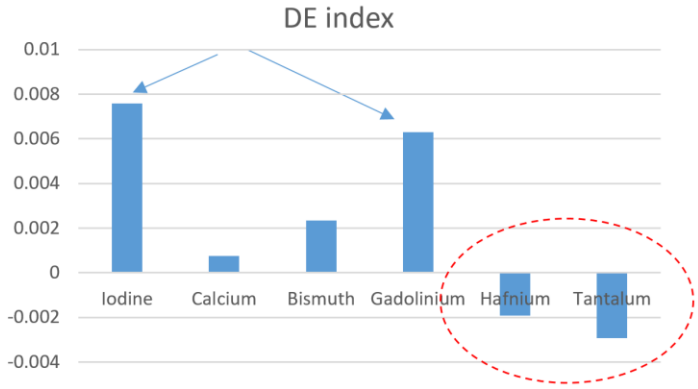

Figure 2: A bar plot of the DE indices shows highest positive values for I and Gd and negative values for Hf and Ta.

1.4 Figures of merit

We have assessed our noise performance by measuring the standard deviation in water vials. The sensitivity of DE CT to particular contrast materials can be quantified by the DE index computed as follows:

$$DE\ index = \frac{XE1-XE2}{XE1+XE2+2000}, \qquad (2)$$

where $XE1, XE2$ are the measured CT numbers normalized by concentration for each element at the two energies. Another figure of merit for material decomposition used here was the condition number of the sensitivity matrix (after unit normalization of each material's sensitivity vector). The condition number is the ratio of the largest and smallest singular values of a matrix, and it quantifies the potential for error amplification when performing matrix inversion (decomposition). A better spectral decomposition would correspond to a lower condition number.

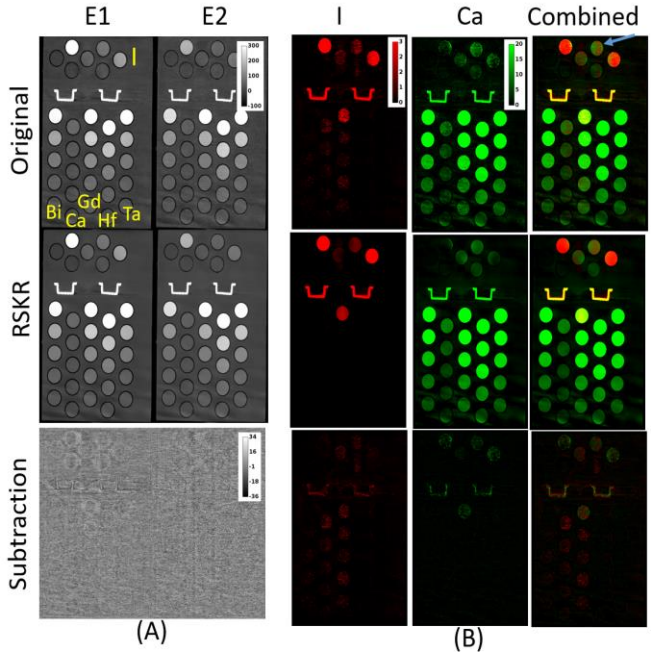

Figure 3: (A) The original, RSKR denoised images and their subtractions for E1 and E2. (B) in-house material decomposition into I (red) and Ca (green) for original and denoised images. We also show the combined color maps and the subtractions.

1.5 Animal Experiments

For the tumor imaging study, we used a carcinogen-induced and genetically engineered primary model of soft tissue sarcoma developed in *p53*$^{fl/fl}$ mice. Primary sarcoma lesions were generated in the hind limb by intramuscular delivery of adenovirus expressing Cre recombinase [9], followed by injection of 300 μg 3-methylcholanthrene (Sigma). Tumors resembling human undifferentiated pleomorphic sarcoma developed approximately 8-12 weeks after injection. Imaging studies were initiated when tumors were palpable (>100 mg). Liposomal-based contrast agents containing iodine (Lip-I) and gadolinium (Lip-Gd) were fabricated similar to methods described previously[10]. Four mice with sarcoma tumors were intravenously injected with Lip-Gd contrast agent (0.32 mg Gd/kg body weight). Three days later (Day 3), the same animals were injected with Lip-I (1.32 mg I/kg body weight) and shortly after they were euthanized. The mice were next immersed in vials with formalin and scanned with both clinical PCCT and PC micro-CT.

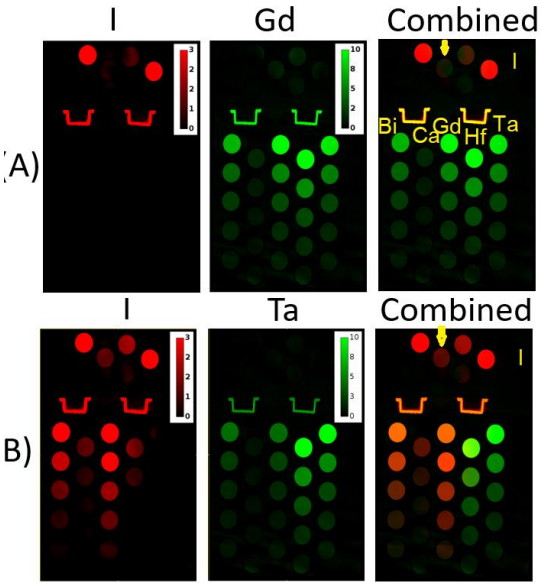

Figure 4. (A) I/Gd and (B) I/Ta decompositions. Note the belter separation of I in the I/Ta decomposition, as predicted by the lower condition number. Note the 1.25 mg/ml I vial (arrow). Hf vials are also very well separated from I. The decompositions were performed on denoised images.

RESULTS

Fig.2 presents the DE indices and shows that I and Gd have the highest values for DE PCCT , and they can be separated best from Bone (Ca). On the other hand, if another material could be used, Hf and Ta show to be best suited as they provide a negative DE index and therefore could be easily separated from either I or Gd. This can be explained by the positions of K-edges i.e. for Ta (67 keV) and Hf (65 keV) relative to the two thresholds. Original reconstructions and RSKR denoising results are shown in Fig. 3. The noise measured in the water vial decreased after RSKR denoising from 8.5 to 2.2 HU for the low energy threshold, E1, and from 10.6 to 2.2 HU for the high energy threshold, E2. Subtraction shows no structural information, thus proving the edge preserving performance. For Ta for example, denoising improved the detectable concentration (Rose criterion, CNR > 5) from 4.5 mg/mL to 1.25 mg/mL for E1 and from 6.5 mg/mL to 1.25 mg/mL for E2. The images were used for I/Ca decomposition (condition number: 11.8).

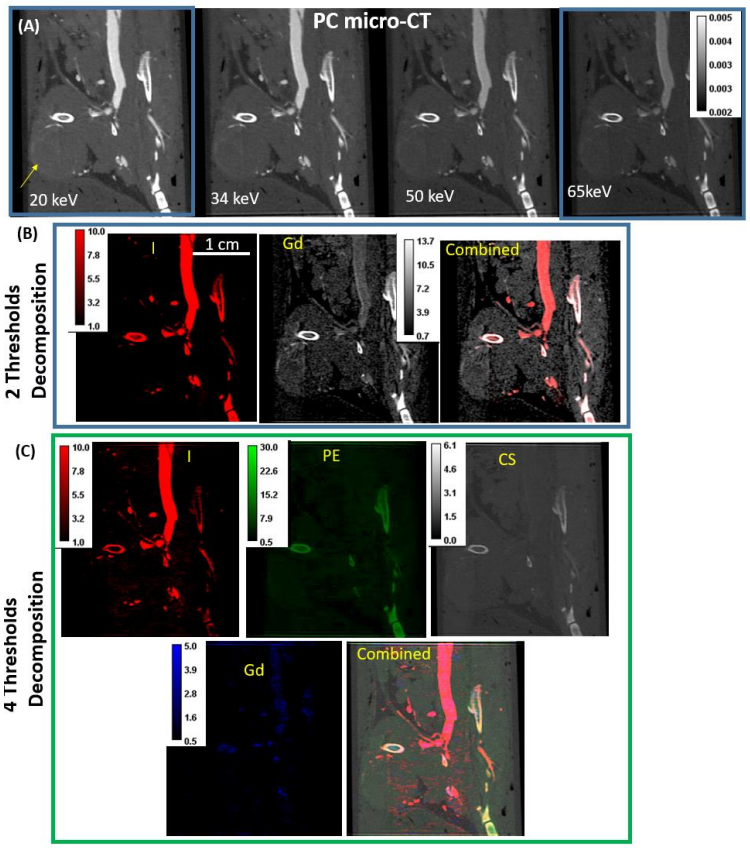

Figure 5: (A) PC micro-CT images of a mouse with a sarcoma tumor reconstructed with 4 energy thresholds. A yellow arrow indicates the tumor. The vasculature is enhanced by the presence of contrast agents. (B) DE decomposition to I/Gd maps and their overlaid display. (C) The I/PE/CS/Gd decomposition using all 4 energy thresholds.

In Fig. 3, the I and Ca maps show levels of cross-contamination for vials of I with concentrations less than 5 mg/ml. Note how denoising improves the decomposition results; however cross-contamination (blue arrow) between I and Ca still exists. Most of the other elements are mapped to the Ca basis. Decomposition images for I/Gd and I/Ta are shown in Fig.4. The condition numbers were 13.63 for I/Gd and 5.14 for I/Ta. As confirmed by Fig.4B, the I/Ta provides the best separation with no significant cross-contamination in the I vials and the best visualization of the low concentration vials.

Fig. 5 presents the results for PC micro-CT in one mouse with a sarcoma tumor. The iterative reconstructions with RSKR ensures similar noise levels in all energy bins (std ~ 20 HU). We show decompositions corresponding to two energy

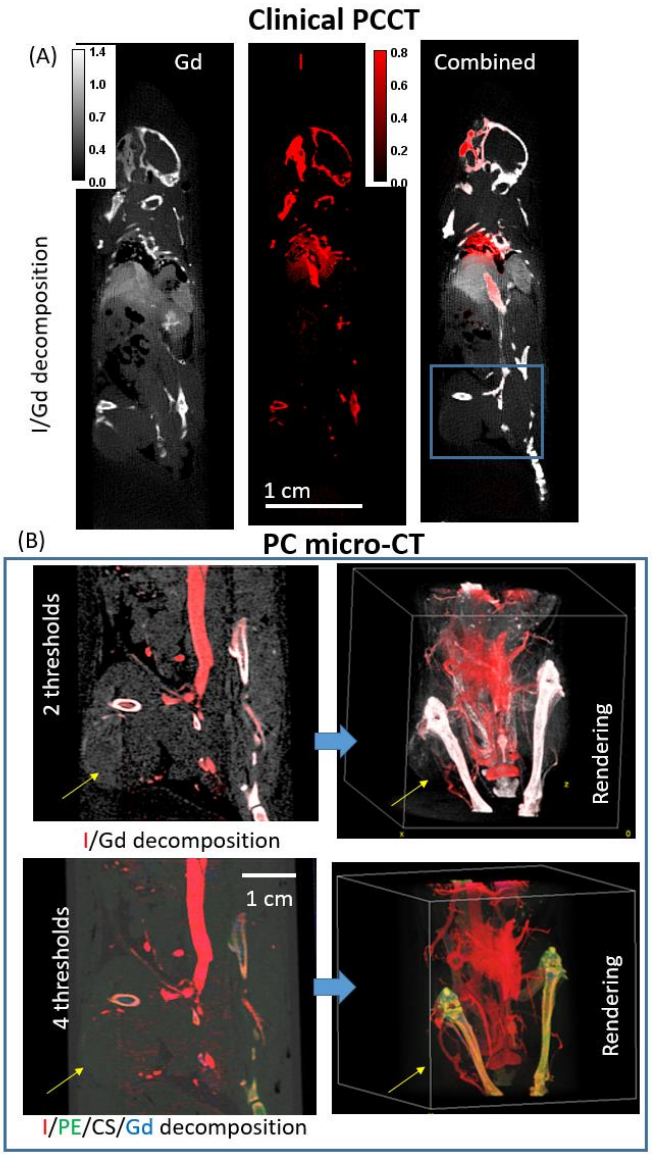

thresholds (20, 65 keV; I/Gd maps) and all four energy thresholds (I, PE, CS, Gd). The tumor appears to contain undetectable Gd levels; however, the vessels containing I are enhanced, and the overall quality of the decomposition is increased when using data corresponding to four energy thresholds.

In Fig. 6 we show a comparison of clinical PCCT and PC micro-CT. The full mouse was scanned with clinical PCCT and the I/Gd decompostion confirms the expected uptake of Gd in the liver and spleen. Note that only the lower part of the body with the tumor was scanned with the PC micro-CT. When using two energy bins, both the clinical and DE PC micro-CT data have been decomposed into I/Gd maps. However, the tumor does not show Lip-Gd accumulation. This may be due to the lower concentration of Gd injected compared to I. Lip-I is present in the vasculature. The cross-contamination between the I and Gd appears to be higher when using DE PC micro-CT data. The four thresholds PC micro-CT data separated into I/PE/CS/Gd shows higher quality and displays smaller vessel in the tumor that is not visible in the DE PC micro-CT rendering (see yellow arrow, Fig. 6).

Finally, in Fig. 7 we show a higher resolution scan of the mouse (voxel size of 0.15x0.15x 0.2 mm) scanned with the clinical PCCT system. The exisiting protocol provides only a single 70 keV VMI image for this setting. RSKR denoising reduces the noise standard deviation from 115 HU to 29HU in soft tissue. Note how the resolution of the clinical PCCT approaches the level of resolution of the PC micro-CT scanner (compare with Fig. 5A).

Figure 6: A comparison of the clinical PCCT (A) and PC micro-CT (B) decompositions using 2 and 4 energy thresholds for the same mouse.

DISCUSSION AND CONCLUSIONS

Our results indicate that Ta (Z=73, K-edge at 67 keV) and Hf (Z=72, K-edge at 65 keV) appear complementary to I and Gd providing excellent candidates for multi-agent studies. Their superior performance is explained by their higher Z number and the proximity of their K-edges to the second threshold (65 keV) of the clinical PCCT scanner. Both Ta [11] and Hf [12] have been proposed as contrast agents for CT imaging. Although current spatial and spectral resolution is lower on the clinical PCCT compared to PC micro-CT, denoising and/or iterative reconstruction can enable spectral imaging at higher resolution and with more than two energies. By performing scans on both clinical and preclinical PC CT we can bridge the translational gap for both imaging algorithms and the developments of new contrast agents including NPs that show promise in the field of cancer theranostics (combined therapy and diagnostics).

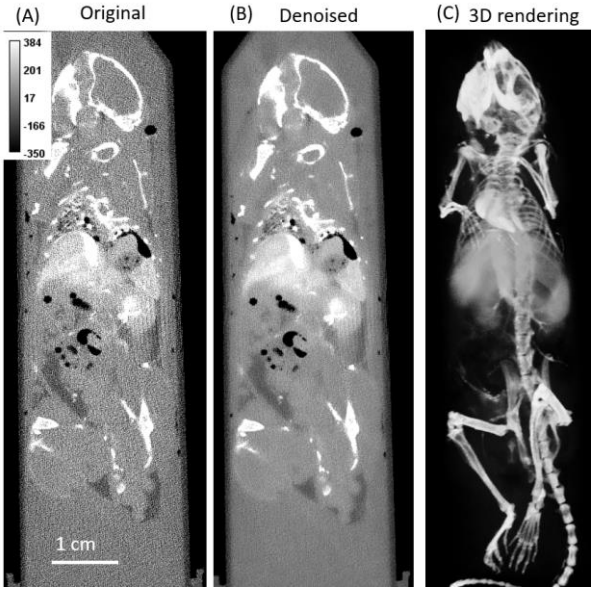

Figure 7: (A) VMI from clinical PCCT. (B) Post-reconstruction denoising using RSKR. (C) A 3D rendering of the denoised set.

ACKNOWLEDGEMENTS

All work was performed at the Quantitative Imaging and Analysis Lab supported by the NIH NIH (R01 CA196667, U24 CA220245, RF1 AG070149);

REFERENCES

[1] R. Symons, B. Krauss, P. Sahbaee *et al.*, "Photon-counting CT for simultaneous imaging of multiple contrast agents in the abdomen: an in vivo study," Medical physics, 44(10), 5120-5127 (2017).

[2] D. P. Cormode, S. Si-Mohamed, D. Bar-Ness *et al.*, "Multicolor spectral photon-counting computed tomography: in vivo dual contrast imaging with a high count rate scanner," Scientific reports, 7(1), 4784 (2017).

[3] M. D. Holbrook, D. P. Clark, and C. T. Badea, "Dual source hybrid spectral micro-CT using an energy-integrating and a photon-counting detector," Phys Med Biol, 65(20), 205012 (2020).

[4] D. P. Clark, M. Holbrook, C. L. Lee *et al.*, "Photon-counting cine-cardiac CT in the mouse," PLoS One, 14(9), e0218417 (2019).

[5] J. R. Ashton, J. L. West, and C. T. Badea, "In vivo small animal micro-CT using nanoparticle contrast agents," Frontiers in pharmacology, 6, 256 (2015).

[6] D. P. Clark, and C. T. Badea, "Hybrid spectral CT reconstruction," PloS one, 12(7), e0180324 (2017).

[7] H. Gao, H. Yu, S. Osher *et al.*, "Multi-energy CT based on a prior rank, intensity and sparsity model (PRISM)," Inverse Probl, 27(11), (2011).

[8] R. E. Alvarez, and A. Macovski, "Energy-selective reconstructions in X-ray computerized tomography," Phys Med Biol, 21(5), 733-44 (1976).

[9] D. G. Kirsch, D. M. Dinulescu, J. B. Miller *et al.*, "A spatially and temporally restricted mouse model of soft tissue sarcoma," Nat Med, 13(8), 992-7 (2007).

[10] S. Mukundan, K. Ghaghada, C. Badea *et al.*, "A Nanoscale, Liposomal Contrast Agent for Preclincal MicroCT Imaging of the Mouse," AJR, submitted, (2005).

[11] J. W. Lambert, Y. Sun, C. Stillson *et al.*, "An Intravascular Tantalum Oxide-based CT Contrast Agent: Preclinical Evaluation Emulating Overweight and Obese Patient Size," Radiology, 289(1), 103-110 (2018).

[12] M. Berger, M. Bauser, T. Frenzel *et al.*, "Hafnium-Based Contrast Agents for X-ray Computed Tomography," Inorg Chem, 56(10), 5757-5761 (2017).